
# Economic Operation Optimization Under Real-Time Pricing for an Energy Management System in a Redundancy-Based Microgrid

Fagundes, Thales Augusto; Fuzato, Guilherme Henrique Favaro; Magossi, Rafael Fernando Quirino; Flores, Manuel Antonio Barrios; Vasquez, Juan C.; Guerrero, Josep M.; Machado, Ricardo Quadros

*Published in:*
IEEE Transactions on Industrial Electronics

*DOI (link to publication from Publisher):*
10.1109/TIE.2023.3325566

*Publication date:*
2024

*Document Version*
Accepted author manuscript, peer reviewed version

# Economic Operation Optimization under Real-Time Pricing for an Energy Management System in a Redundancy-Based Microgrid

Thales Augusto Fagundes, Guilherme Henrique Favaro Fuzato, *Member, IEEE*, Rafael Fernando Quirino Magossi, Manuel Antonio Barrios Flores, Juan C. Vasquez, *Senior Member, IEEE*, Josep M. Guerrero, *Fellow, IEEE*, and Ricardo Quadros Machado, *Senior Member, IEEE*

***Abstract*—DC microgrids (MGs) represent self-contained systems for distributing and managing electricity locally, offering advantages in terms of efficiency and control. This paper proposes the optimization of redundancy-based dc MG, emphasizing the integration of an intelligent algorithm to minimize operational costs under real-time pricing conditions and also increase the efficiency operation. The redundancy-based dc MG consists of a cascaded bidirectional Cuk converter (CBC) linked to a cascaded bidirectional boost converter (CBB), sharing two battery energy storage system (BESS) units as common inputs. Thereby, two boost converters interface the dc utility and FC to the dc-link of the CBC. The redundancy-based dc MG operates with a coordinated and decentralized control among the dc utility, fuel cell (FC) and two BESS units. The energy management system (EMS) employs droop control for the dc utility and FC, while BESS units adhere to a state-of-charge (SoC)-Sharing function. Additionally, the particle swarm optimization (PSO) dynamically adjusts EMS parameters for optimal real-time performance. Then, a stability analysis determines MG operational boundaries, and the effectiveness of the method is confirmed through experiments using Typhoon HIL and dSPACE setups. Finally, comparative evaluations against traditional SoC based droop and Genetic Algorithms (GA) demonstrate the cost reduction of the proposed approach.**

***Index Terms*—battery energy storage system (BESS), energy management system (EMS), operating cost, particle swarm optimization (PSO), state-of-charge (SoC) equalization.**

## I. Introduction

This work was supported by the Coordination for the Improvement of Higher Education Personnel (CAPES) under grants PDSE-88881.187771/2018-01 and 88881.030370/2013-0, the National Council for Scientific and Technological Development (CNPq) under grant 312664/2021-4 and the São Paulo Research Foundation (FAPESP) under grants 2013/20721-4, 2020/05865-3 and 2022/02721-6.

T. A. Fagundes and R. Q. Machado are with the São Carlos School of Engineering, University of São Paulo, São Carlos SP 13566-590, Brazil (e-mail: thales.fagundes@usp.br; rquadros@sc.usp.br).

G. H. F. Fuzato is with the Federal Institute of Education, Science and Technology of São Paulo, Campinas SP 01109-010, Brazil (e-mail: guilherme.fuzato@ifsp.edu.br).

R. F. Q. Magossi is with Solar21, São Paulo, Brazil (e-mail: rafael.magossi@solar21.com.br).

M. A. B. Flores, J. C. Vasquez and J. M. Guerrero are with the Department of Energy Technology, University of Aalborg, 9220 Aalborg, Denmark (e-mail: mabf@energy.aau.dk; juq@energy.aau.dk; joz@energy.aau.dk).

AS the employment of renewable energy sources (RES) has grown to reduce the negative impact of pollution produced by conventional power plants that use fossil fuels, several studies have proposed methods to enhance the operation of RES connected to power converters in dc microgrids (MGs). Consequently, the power flow coordination is managed through the energy management system (EMS), while the optimization process ensures that the MG operates at an optimized operating point [1]. In the context of EMS, droop control techniques were employed to regulate the dc-link voltage in [2]. As a result, the droop control stabilizes the grid voltage in the primary control, while the power balance is restored after uncertain events in the secondary control level [3], and the tertiary control layer coordinates power flow using the EMS [4].

Furthermore, the state-of-charge (SoC) based droop is crucial for effectively managing the energy transfer within the battery energy storage system (BESS) units in a MG. It ensures the SoC equalization and prevents unpredictable charge/discharge rates that could potentially decrease battery lifespan, as highlighted in [5]. In line with this, the work in [6] proposed a traditional SoC based droop approach incorporating a modified virtual resistance as an SoC function, while in [7], a Fuzzy controller is introduced to integrate the virtual resistance into the SoC based droop approach. Additionally, [8] implemented a scaling coefficient by weighting the SoC.

Importantly, the focus is not only on modifying the coefficients of the virtual resistance in a droop control to achieve SoC balancing among the BESS units. Alternatives include a sigmoid function, as proposed in [5], and a Fuzzy controller which coordinated the power flow through the dc-link, as discussed in [9]. Nevertheless, in terms of SoC equalization, economic dispatch specific to BESS operation and concerns related to minimizing energy losses in dc MGs were not addressed in [5], [7]–[10].

Conversely, numerous strategies have been explored to enhance the optimal functioning of a MG, taking into account objectives such as minimizing energy losses, implementing economic dispatch, and improving load balancing. For instance, a cost-effective solution was implemented in [11] using a genetic algorithm (GA) within a droop control six-bus dc MG. However, aspects regarding SoC equalization were not

addressed in this study. Similarly, a distributed optimal control technique was introduced in [12] to mitigate operational losses and maintain stable the dc-link voltage in a dc MG using the Karush–Kuhn–Tucker conditions, although this type of solution did not involve any application based on the BESS units.

Concerning [13], the economic dispatch employed the Lagrange multipliers approach but omitted SoC balancing among BESS units. Conversely, [14] proposed the use of a particle swarm optimization (PSO) to determine optimal parameters for a virtual-battery model, with the objective of minimizing daily operating costs within a dc MG. Remarkably, this approach took into account SoC equalization within a conventional dc MG structure. Lastly, [15] focused on implementing a pure voltage-based optimal control method in a dc MG, where there was a lack of BESS applications.

In the context of dc MG structures, most optimization problems were applied to generic models, such as multiple sources connected to a common dc-link [14], or multiple buses [11], [12], [15]. However, the topology of dc/dc converters, which impacts the performance, was often overlooked. Redundancy in power converter structures addresses the challenges of unpredictable operation in shipboards [16] and also ensures the operation of military, aerospace systems, and healthcare devices [17]. In addition, parallel modules in dc/dc converters are crucial for improving reliability in dc MGs coordinated by an EMS, as mentioned in [18]. For instance, [19] addressed the EMS in a redundant hybrid dc MG, while [20] proposed a multilevel bidirectional dc/dc converter for shipboard applications. However, there are no optimization strategies related to EMS parameters in [19], [20].

Accordingly, this paper presents a solution for an optimization problem that considers the operating cost of the fuel cell (FC), dc utility and the BESS units in a redundancy-based dc MG. Thus, the EMS employs the droop control to manage the FC and dc utility, and it utilizes the SoC-Sharing function to balance the SoC among the BESS units, with their parameters (droop control and SoC-Sharing function) modified by the PSO technique according to the real-time pricing of electricity and hydrogen ($H_2$). In this context, Fig. 1 defines the redundancy-based dc MG, which connects each BESS unit into two distinct common inputs, along with two boost converters to integrate the FC and the dc utility into the main dc-link. Additionally, Fig. 2 illustrates the redundancy arrangement composed of a cascaded bidirectional Cuk converter (CBC) and a cascaded bidirectional boost converter (CBB).

Since real-time measurements from the redundancy-based dc MG are sent directly to the PSO, the CBC is suitable for calculating the power demanded on the main dc-link within a specific time range defined by the PSO algorithm. Furthermore, the CBB equalizes the BESS units using a battery-to-battery (B2B) method through the secondary dc-bus. Additionally, the redundancy accomplished through the CBC and CBB is suitable for maximizing the BESS operation and also reducing the operating cost of the FC and dc utility when the parameters of the SoC-Sharing function are adjusted by the PSO.

The authors also analyze the stability of the redundancy-based dc MG by employing Lyapunov's indirect method as applied by [21]. Therefore, the redundancy-based dc MG average model is defined by coupling the CBC, CBB and the two boost converters used as interfaces on the FC and the dc utility terminals via dc-link, with the CBB and CBC incorporated as one single power structure.

Finally, as the objective is to assess the behavior of SoC and current dynamics in a redundancy-based dc MG, it is assumed that the State-of-Health (SoH) is the same for each BESS. Therefore, BESS units operating with similar SoC levels degrade their SoH equally, as indicated in [22]. Additionally, the SoC-Sharing function optimized via PSO is compared with the SoC based droop, also optimized by the PSO, as well as the SoC-Sharing function optimized via GA.

Accordingly, the main contributions of the paper are described as follow.

1) By incorporating redundancy into the dc MG, the reliability and stability of the system can be increased. This is achieved by dividing the BESS currents, while considering the economic cost of operation and adhering to the constraints of the redundancy-based dc MG;
2) EMS parameters are integrated into a real-time optimization algorithm based on economic dispatch;
3) A cost-effective strategy that considers a redundancy-based dc MG and SoC equalization for BESS units.

The paper is structured as follows: Section II discusses the proposed redundancy-based dc MG. Section III explains the EMS with the droop control and SoC-Sharing function modified by PSO. In Section IV, the optimization problem with the operating cost is addressed. In Section V, the stability analysis using Lyapunov's indirect method is presented. The experimental results of the EMS operating with PSO are shown in Section VI. Lastly, the paper concludes with Section VII.

## II. System Description

The proposed redundancy-based dc MG presented in Fig. 1 consists of CBC and CBB modules. The FC and dc utility are connected to the dc-link through boost converters, while BESS1 and BESS2 are tied to the CBC and CBB inputs. In the same picture, $v_{fc}$, $v_{utility}$, $v_{bat1}$, and $v_{bat2}$ represent the voltages at the FC, dc utility, BESS1, and BESS2 terminals, respectively. The corresponding currents supplied by them are denoted as $i_{fc}$, $i_{utility}$, $i_{bat1}$, and $i_{bat2}$. In this way, $R_o$ represents the dc load connected to the CBC dc-link, while the inductance currents through $L_1$, $L_2$, $L_3$, $L_4$, $L_5$, and $L_6$ are denoted as $i_{L1}$, $i_{L2}$, $i_{L3}$, $i_{L4}$, $i_{L5}$, and $i_{L6}$, respectively, with $i_{bat1} = i_{L1} + i_{L5}$ and $i_{bat2} = i_{L3} + i_{L6}$.

The CBC dc-link capacitance with terminal voltage $v_o$ is $C_o$, and $C_3$ represents the secondary bus capacitance with voltage $v_{C3}$ measured at the CBB output. The capacitance $C_1$ receives energy from BESS1, and $C_2$ receives energy from BESS2, with the voltages $v_{C1}$ and $v_{C2}$ computed at their respective terminals. Both bidirectional topologies utilize controlled semiconductors $S_1$, $S_2$, $S_3$, and $S_4$ (direct command), as well as $\bar{S}_1$, $\bar{S}_2$, $\bar{S}_3$, and $\bar{S}_4$ (complementary command), driven by classical PWM, as shown in Fig. 2.

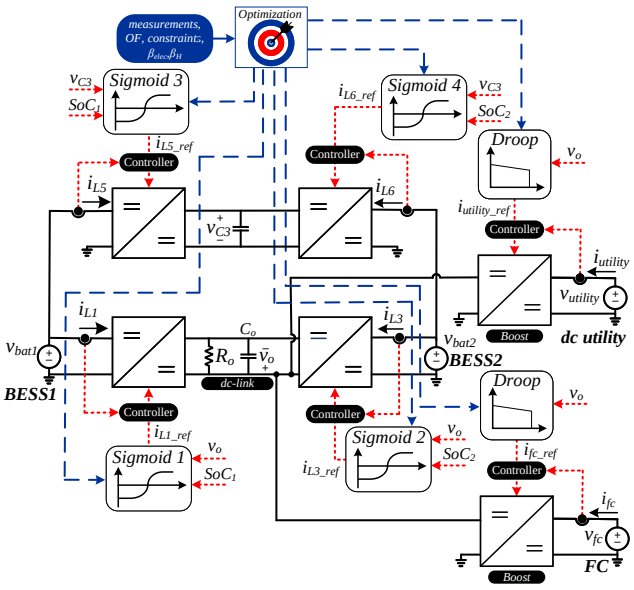


Fig. 1. Optimal EMS designed to the redundancy-based dc MG.

## III. EMS Methodology

The EMS proposed in [5] coordinates BESS1, BESS2, FC, and dc utility in a decentralized manner. It balances $SoC_1$ and $SoC_2$ of BESS1 and BESS2, and supplies power to the dc load connected to the dc-link.

### A. System Control

The current references, denoted as $i_{L1\_ref}$ and $i_{L3\_ref}$, are defined by two SoC-Sharing functions using Sigmoid 1 and Sigmoid 2. These SoC-Sharing functions take $SoC_1$, $SoC_2$, and $v_o$ as inputs to process current references for both inductances. Additionally, the voltage $v_{C3}$, combined with $SoC_1$ and $SoC_2$, provides $i_{L5\_ref}$ and $i_{L6\_ref}$ using Sigmoid 3 and Sigmoid 4, respectively. Subsequently, the current references ($i_{L1\_ref}$, $i_{L3\_ref}$, $i_{L5\_ref}$, and $i_{L6\_ref}$) are compared to the measured inductance currents ($i_{L1}$, $i_{L3}$, $i_{L5}$, and $i_{L6}$), with the resulting values processed through the PI controllers. It is important to emphasize that PI tuning is crucial for achieving a rapid response from current steps during the optimization process.

In the context of the the FC and dc utility, a classical droop controller is employed on the FC management to determine $i_{fc\_ref}$, taking the voltage $v_o$ as its input. Similarly, the dc utility management employs another droop control, also utilizing $v_o$ as input to calculate $i_{utility\_ref}$. Later, the measured currents, namely $i_{fc}$ and $i_{utility}$, are compared with their references. Finally, the results are then processed through their respective PI controllers to produce their duty-cycles.

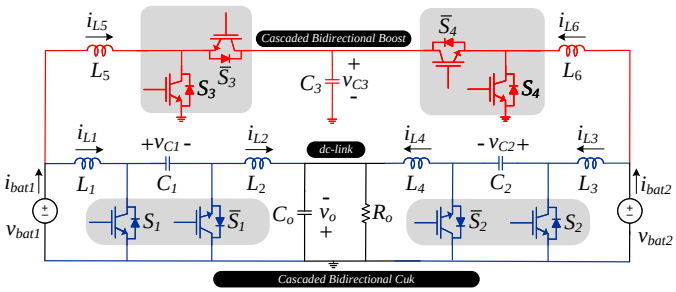


Fig. 2. BESS1 and BESS2 connected to the CBC and CBB.

### B. Optimal Droop Control

The authors propose a droop control, optimized by the PSO, to produce the current reference $i_{source\_ref}$. This reference takes the form of $i_{fc\_ref}$ for the FC and $i_{utility\_ref}$ for the dc utility, as defined in (1).

$$i_{source\_ref} = \overbrace{\alpha_{droop}}^{PSO}\underbrace{\left(-\frac{v_o}{\Delta v}+\frac{\overbrace{v_{DC0}}^{PSO}+\Delta v}{\Delta v}\right)}_{term\ in\ p.u.} \tag{1}$$

where $v_o$ is the dc-link voltage (although the Cuk's terminal voltage is negative, the voltage sensor provides the absolute value of the measured voltage), and $\Delta v$ is its voltage range.

The PSO algorithm modifies two key parameters in the mathematical model defined by (1), namely $\alpha_{droop}$ and $v_{DC0}$. The parameter $\alpha_{droop}$ determines the maximum current that the source can supply by multiplying the per unit (p.u.), while $v_{DC0}$ affects the minimum dc-link voltage. Additionally, the PSO algorithm adjusts both parameters to optimize redundancy-based dc MG performance and maximize the power production from each source.

Fig. 3(a) illustrates the optimal droop control and its impact on the virtual resistance, which is calculated as $r_{virtual} = \Delta v/\alpha_{droop}$, considering the influence of $\alpha_{droop}$ and $v_{DC0}$.

### C. Optimal SoC-Sharing Function

The definition for the SoC-Sharing function is provided in [5], and it is subsequently implemented in this study within a redundancy-based dc MG. Thus, the currents reference from the inductances $L_1$, $L_3$, $L_5$ and $L_6$ are calculated considering the mathematical model shown in (2).

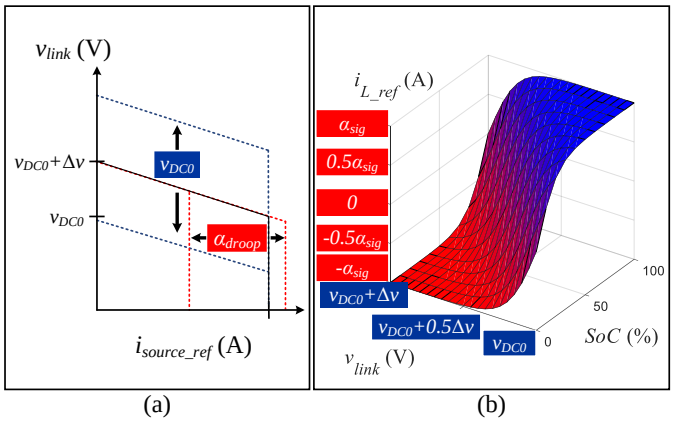


Fig. 3. PSO parameters: (a) modifying the droop control and (b) the SoC-Sharing function.

$$\begin{cases} i_{L\_ref} = \overbrace{\alpha_{sig}}^{PSO} \underbrace{\left( \dfrac{2}{1 + e^{(e_{factor} - \mathrm{SoC})10}} - 1 \right)}_{term\ in\ p.u.} \\ e_{factor} = \dfrac{v_{link} - \overbrace{v_{DC0}}^{PSO}}{\Delta v} \end{cases} \quad (2)$$

where $e_{factor}$ is the equalization factor and SoC is $\mathrm{SoC}_1$ on Sigmoid 1 and Sigmoid 3, while Sigmoid 2 and Sigmoid 4 receive $\mathrm{SoC}_2$ as input. In (2), $v_{link}$ is the dc-link voltage with $v_o$ for CBC and $v_{C3}$ for CBB, $v_{DC0}$ is the minimum voltage on dc-link according to CBB and CBC, while $\Delta v$ is the voltage range. Additionally, the SoC-Sharing function was plotted in Fig. 3(b) using 3-D reference frames, where the current reference $i_{L\_ref}$ is evaluated considering the dc-link voltage $v_{link}$ and the SoC from the BESS. According to this picture and (2), the parameters $\alpha_{sig}$ and $v_{DC0}$, which are used in the SoC-Sharing function, are also addressed in the PSO algorithm, thereby modifying the behavior of the SoC-Sharing function.

For instance, Fig. 4 indicates the SoC-Sharing function in relation to $i_{L\_ref}$ (from -1 to 1 p.u.) and $v_{link}$ (from 200 to 215 V), considering the EMS when the BESS has SoC levels of 0%, 25%, 50%, 75% and 100%. As a result, if the BESS is completely discharged (SoC lower than 25%), the current reference is responsible for charging the BESS according to the dc-link, except in cases of substantial power demand. Conversely, when the BESS is fully charged, the algorithm works to provide power according to the dc load demand. Thus, the SoC-Sharing function can also play a crucial role in managing the SoC limitations within the redundancy-based dc MG.

Concerning Sigmoid 1 and Sigmoid 2 on CBC, the modified PSO parameters are $\alpha_{sig\_cuk}$ and $v_{DC0\_o}$ for the main dc-link, while Sigmoid 3 and Sigmoid 4 on CBB receive $\alpha_{sig\_boost}$ and $v_{DC0\_C3}$ for the secondary dc-bus. As (2) has a term defined in p.u., $\alpha_{sig\_cuk}$ is responsible to define the amount of power on CBC, while $\alpha_{sig\_boost}$ specifies the amount of power on CBB. Furthermore, $v_{DC0\_o}$ is the same parameter for the droop control which can define the minimum voltage on the main dc-link (on $C_o$), while $v_{DC0\_C3}$ can set the minimum voltage on the capacitance $C_3$ according to the SoC equalization.

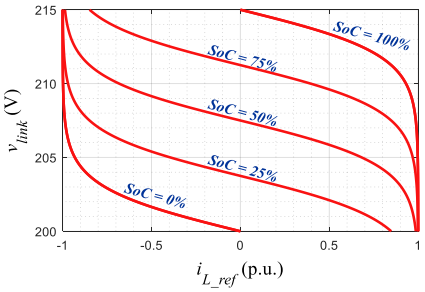


Fig. 4. SoC-Sharing function considering the relationship between $v_{link}$ and $i_{L\_ref}$ according to the BESS SoC-level.

## IV. Optimization Problem

Optimization is extensively employed to address operational challenges within MG systems by identifying the most viable solutions [23]. However, due to the presence of various nonlinear elements in dc MGs, such as dc/dc converters, dynamic response of FCs and BESS units during charging and discharging, the optimization problems associated with them are categorized as non-convex. Consequently, evolutionary and particle swarm intelligence exhibit suitability for optimizing the operation of the redundancy-based dc MG. In this context, the PSO stands out as a well-known technique within swarm intelligence, while GA holds a prominent position among population-based meta-heuristic algorithm founded on the evolutionary process [1].

The benefits of PSO in comparison to GA encompass its simpler implementation requiring fewer tuning parameters, its adeptness in retaining valuable information, and its efficiency in preserving swarm diversity [24]. Therefore, the PSO is a computational strategy inspired by bird flocking and fish schooling behavior, aiming to find the best solution for a given problem. It involves updating the particle swarm in the search-space based on the mathematical operations involving particle position and velocity. Initially, particle positions are randomly generated, and their velocities are updated according to their positions and the best cost obtained from the objective function. Consequently, the particles move around the best-known position in the search-space [25].

Therefore, the optimization structure designed to provided the best parameters (particle position of PSO) to the EMS are: $v_{DC0\_o}$, $v_{DC0\_C3}$, $\alpha_{sig\_cuk}$, $\alpha_{sig\_boost}$, $\alpha_{droop\_fc}$ and $\alpha_{droop\_utility}$. Thus, the dc-link voltage $v_o$ is influenced by $v_{DC0\_o}$ variation, while $v_{C3}$ is impacted by changing $v_{DC0\_C3}$. Moreover, $\alpha_{sig\_cuk}$ defines the equalization current on CBC by modifying Sigmoid 1 and Sigmoid 2, while $\alpha_{sig\_boost}$ impacts Sigmoid 3 and Sigmoid 4 designed to CBB. Finally, the droop controllers on the FC and dc utility are adjusted by $\alpha_{droop\_fc}$ and $\alpha_{droop\_utility}$, respectively.

### A. Objective Function

The PSO receives from the lower level of control the average currents $I_{L1}$, $I_{L3}$, $I_{L5}$ and $I_{L6}$ from the inductances, the average voltages $V_{bat1}$ and $V_{bat2}$ from BESS units, the average dc currents and voltages $I_{utility}$, $V_{utility}$, $I_{fc}$ and $V_{fc}$ from dc sources and the average power demanded on the main dc-link $P_{load}$ within a specified time interval $\Delta t_{opt}$.

In addition, the redundancy-based dc MG cost is obtained by the cost of the power flow through the BESS units ($Z_{bat1}$ and $Z_{bat2}$), the FC ($Z_{fc}$), the dc utility ($Z_{utility}$) and the MG power losses ($Z_{loss}$). Then, the main objective of PSO is to reduce the operational cost of dispatchable units according to the real-time pricing by using the objective function (OF) defined in (3) and described in [11].

After the process of data acquisition/transference within the $\Delta t_{opt}$ time frame to process the average information, the PSO is turned-on to minimize the OF. To achieve the aforementioned targets, the total costs are calculated according to the real-time generation fees for electricity ($\beta_{elec}$) and $H_2$

cost ($\beta_{H_2}$). In sequence, the optimal parameters are adjusted to decrease the operational expenses from the redundancy-based dc MG, while also adhering to technical constraints.

$$minimize \;\; OF = Z_{bat1} + Z_{bat2} + Z_{fc} + Z_{utility} + Z_{loss} \tag{3}$$

### B. Cost Assigned to the BESS

The operating cost of the BESS has the influence from the battery charging efficiency ($\eta_{ch}$), discharging efficiency ($\eta_{dis}$), the real-time pricing of electricity ($\beta_{elec}$) and the BESS power, as can be defined in (4).

$$Z_{bat} = \begin{cases} \beta_{elec}\left(\frac{P_{bat}(\eta_{ch}-1)}{\Delta T}\right), P_{bat} < 0 \\ \beta_{elec}\left(\frac{P_{bat}(1-1/\eta_{dis})}{\Delta T}\right), P_{bat} > 0 \end{cases} \tag{4}$$

where $P_{bat}$ is the BESS power, while $\Delta T$ identifies the number of PSO steps in one hour.

### C. Cost Assigned to the FC

The FC cost assigned to this type of alternative energy source can be defined according to the $H_2$ consumption, and it is related with the power at its terminals, as shown in (5). In this expression, the FC average current is $I_{fc}$, the average voltage is defined by $V_{fc}$, while $a_{fc}$ and $b_{fc}$ represent the fuel consumption in the FC and $\beta_{H_2}$ the real-time pricing of $H_2$.

$$Z_{fc} = \beta_{H_2}\left(\frac{a_{fc}(V_{fc}I_{fc})^2 + b_{fc}(V_{fc}I_{fc})}{\Delta T}\right) \tag{5}$$

### D. Utility Power Cost

The dc utility is held as the source that can provided power to the grid according to the market price, which cost is defined in (6), where $V_{utility}$ and $I_{utility}$ correspond to the average voltage and current at the grid terminals.

$$Z_{utility} = \beta_{elec}\left(\frac{V_{utility}I_{utility}}{\Delta T}\right) \tag{6}$$

### E. Cost of the Power Losses

By analyzing the power flow during the redundancy-based dc MG operation, the cost of the power losses can be calculated according to (7). In this mathematical solution, the average power through the FC, the dc utility, produced/absorbed by the BESS units and demanded by the load are $P_{fc}$, $P_{utility}$, $P_{bat1}$, $P_{bat2}$ and $P_{load}$, respectively.

$$Z_{loss} = \beta_{elec}\left(\frac{P_{fc}+P_{utility}+P_{bat1}+P_{bat2}-P_{load}}{\Delta T}\right) \tag{7}$$

### F. Constraints

The constraints are important to restrict the solution of the optimization problem by setting conditions according to the limits of operation in which the redundancy-based dc MG works. Thus, a penalty is added to the operating cost if some boundary are exceeded. Therefore, as the redundancy-based dc MG operates with EMS, there is no need for equality constraints. The constraints based on the inequalities, defined in (8), are crucial to achieve the aforementioned requirements, where $I_{bat}^{min}$ represents the lower limit of current and $I_{bat}^{max}$ represents the upper limit of current for the BESS. Subsequently, the BESS is able to operate within a secure operational SoC range by imposing constraints of SoC based on $SoC^{min}$ and $SoC^{max}$, along with the power gradient limitation $\nabla P_{bat} = P_{bat} - P_{bat}(t+1)$ [26].

Additionally, the minimum values for the dc-link average voltages $V_o$ and $V_{C3}$ are $V_o^{min}$ and $V_{C3}^{min}$, while the maximum values are $V_o^{max}$ and $V_{C3}^{max}$. The average power produced by the FC has to be inside the interval $P_{fc}^{min}$ and $P_{fc}^{max}$, while the average power supplied by the dc utility between $P_{utility}^{min}$ and $P_{utility}^{max}$. Moreover, the FC and dc utility must operate with their power coordinated between $\xi^{min}$ and $\xi^{max}$, while the average power on the dc load terminals has to be no greater than the upper limit $P_{load}^{max}$ and no inferior than the lower limits $P_{load}^{min}$. Finally, the PSO parameters have the following lower limits: $V_{DC0\_o}^{min}$, $V_{DC0\_C3}^{min}$, $\alpha_{sig\_cuk}^{min}$, $\alpha_{sig\_boost}^{min}$, $\alpha_{droop\_fc}^{min}$, $\alpha_{droop\_utility}^{min}$, while the upper limits are $V_{DC0\_o}^{max}$, $V_{DC0\_C3}^{max}$, $\alpha_{sig\_cuk}^{max}$, $\alpha_{sig\_boost}^{max}$, $\alpha_{droop\_fc}^{max}$, $\alpha_{droop\_utility}^{max}$.

$$\begin{cases} I_{bat}^{min} \le I_{bat} \le I_{bat}^{max} \\ SoC^{min} \le SoC \le SoC^{max} \\ |\nabla P_{bat}| \le \Delta P_{bat} \\ V_o^{min} \le V_o \le V_o^{max} \\ V_{C3}^{min} \le V_{C3} \le V_{C3}^{max} \\ P_{fc}^{min} \le P_{fc} \le P_{fc}^{max} \\ P_{utility}^{min} \le P_{utility} \le P_{utility}^{max} \\ \xi^{min} \le P_{utility} + P_{fc} \le \xi^{max} \\ P_{load}^{min} \le P_{load} \le P_{load}^{max} \\ V_{DC0\_o}^{min} \le V_{DC0\_o} \le V_{DC0\_o}^{max} \\ V_{DC0\_C3}^{min} \le V_{DC0\_C3} \le V_{DC0\_C3}^{max} \\ \alpha_{sig\_cuk}^{min} \le \alpha_{sig\_cuk} \le \alpha_{sig\_cuk}^{max} \\ \alpha_{sig\_boost}^{min} \le \alpha_{sig\_boost} \le \alpha_{sig\_boost}^{max} \\ \alpha_{droop\_fc}^{min} \le \alpha_{droop\_fc} \le \alpha_{droop\_fc}^{max} \\ \alpha_{droop\_utility}^{min} \le \alpha_{droop\_utility} \le \alpha_{droop\_utility}^{max} \end{cases} \tag{8}$$

### G. Operation of the PSO

The PSO flowchart is presented in Fig. 5, where a random solution is generated with the particle position being the parameters provided to the EMS. After the time step of the PSO, the average currents and voltages (in accordance with the $\Delta t_{opt}$ time frame) from the redundancy-based dc MG are calculated, and used to evaluate the total operating cost, taking into account the real-time pricing of electricity, the cost of $H_2$, and the penalty for each constraints violation.

Additionally, if the calculated total cost is lower than the local best cost produced in the swarm size (PSO population) and the global best solution, then these values are updated as a new total cost. Subsequently, the velocity and particle position are adjusted based on the updated local and global best positions, where the particle position represents the parameters updated in the EMS operation. Finally, the performance of PSO continues until the specified number of iterations is achieved; then, the global best solution remains as the EMS parameters. For instance, the best cost regarding the iterative

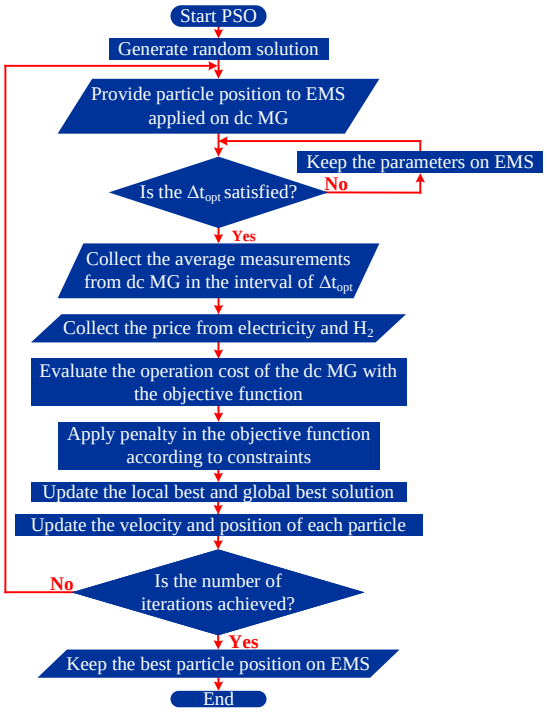


Fig. 5. Flowchart of the PSO.

cycles is evaluated, as exemplified in Fig. 6, and then the best parameters are maintained in the EMS.

## V. Stability Analysis

The Lyapunov's indirect method was applied to verify the operation stability of the EMS employed in the dc MG according to [21]. The interaction among dc utility and FC converters, CBC, CBB and their controllers is represented in (9).

$$\begin{bmatrix} \dot{v}_o \\ \dot{\boldsymbol{x}}_{cb}^{(1:9)} \\ \dot{e}_{iL1} \\ \dot{e}_{iL3} \\ \dot{e}_{iL5} \\ \dot{e}_{iL6} \\ \dot{\boldsymbol{x}}_{fc}^{(1:2)} \\ \dot{e}_{fc} \\ \dot{\boldsymbol{x}}_{utility}^{(1:2)} \\ \dot{e}_{utility} \end{bmatrix} = \begin{bmatrix} dc_{coupled} \\ \boldsymbol{A_{cb}}(k_1,k_2,k_3,k_4)^{(1:9,1:10)}\boldsymbol{x_{cb}} + \boldsymbol{B_{cb}}(k_1,k_2,k_3,k_4)^{(1:9,1:2)}\boldsymbol{u_{cb}} \\ i_{L1\_ref} - Hi_{L1}i_{L1} \\ i_{L3\_ref} - Hi_{L3}i_{L3} \\ i_{L5\_ref} - Hi_{L5}i_{L5} \\ i_{L6\_ref} - Hi_{L6}i_{L6} \\ (\boldsymbol{A}_{fc10}^{(1,1:2)} + k_{fc}\boldsymbol{A}_{fck}^{(1,1:2)})\boldsymbol{x}_{fc} + (\boldsymbol{B}_{fc0}^{(1,1)} + k_{fc}\boldsymbol{B}_{fck}^{(1,1)})\boldsymbol{u}_{fc} \\ i_{fc\_ref} - Hi_{fc}i_{fc} \\ (\boldsymbol{A}_{utility10}^{(1,1:2)} + k_{utility}\boldsymbol{A}_{utilityk}^{(1,1:2)})\boldsymbol{x}_{utility} + \boldsymbol{B}_{utility0}^{(1,1)} + k_{utility}\boldsymbol{B}_{utilityk}^{(1,1)})\boldsymbol{u}_{utility} \\ i_{utility\_ref} - Hi_{utility}i_{utility} \end{bmatrix} \quad (9)$$

Additionally, the term:

$$\begin{aligned} dc_{coupled} =& (\boldsymbol{A}_{cb}(k_1,k_2,k_3,k_4)^{(10,1:10)})\boldsymbol{x}_{cb} + (\boldsymbol{B}_{cb}(k_1,k_2,k_3,k_4)^{(10,1:10)})\boldsymbol{u}_{cb}\ldots \\ &\cdots - (\boldsymbol{A}_{fc0}^{(2,1:2)} + k_{fc}\boldsymbol{A}_{fck}^{(2,1:2)})\boldsymbol{x}_{fc} - (\boldsymbol{B}_{fc0}^{(2,1)} + k_{fc}\boldsymbol{B}_{fck}^{(2,1)})\boldsymbol{u}_{fc}\ldots \\ &\cdots - (\boldsymbol{A}_{utility0}^{(2,1:2)} + k_{utility}\boldsymbol{A}_{utilityk}^{(2,1:2)})\boldsymbol{x}_{utility} - (\boldsymbol{B}_{utility0}^{(2,1)} + k_{utility}\boldsymbol{B}_{utilityk}^{(2,1)})\boldsymbol{u}_{utility}\ldots \\ &\cdots + \left(2\tfrac{v_o}{R_oC_o}\right). \end{aligned}$$

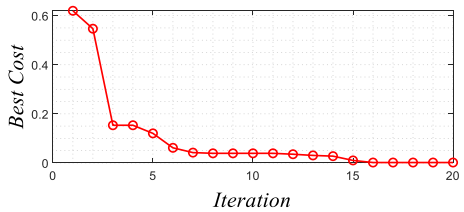


Fig. 6. Example of best cost vs. iterative cycles.

specifies the influence of all power converters in the main dc-link $v_o$.

Thereby, the movement of the eigenvalues is evaluated according to the Jacobian's matrix. From (9), the state and input vectors of the CBC and CBB, modelled as one topology, are $\boldsymbol{x}_{cb} = \begin{bmatrix} i_{L1} & i_{L2} & v_{C1} & i_{L3} & i_{L4} & v_{C2} & i_{L5} & i_{L6} & v_{C3} & v_o \end{bmatrix}^T$ and $\boldsymbol{u}_{cb} = \begin{bmatrix} v_{bat1} & v_{bat2} & v_o \end{bmatrix}^T$. In addition, the state and input vectors of the dc utility and FC are $\boldsymbol{x}_{fc} = \begin{bmatrix} i_{fc} & v_o \end{bmatrix}^T$, $\boldsymbol{x}_{utility} = \begin{bmatrix} i_{utility} & v_o \end{bmatrix}^T$, $\boldsymbol{u}_{fc}$ and $\boldsymbol{u}_{utility}$, while the error of currents from the PI controllers are $\dot{\boldsymbol{e}}_{iL1}$, $\dot{\boldsymbol{e}}_{iL3}$, $\dot{\boldsymbol{e}}_{iL5}$, $\dot{\boldsymbol{e}}_{iL6}$, $\dot{\boldsymbol{e}}_{fc}$ and $\dot{\boldsymbol{e}}_{utility}$.

Regarding the state space, from the model illustrated in Fig. 2 and (9), it is defined the weighted matrix $\boldsymbol{A}_{cb}(k_1,k_2,k_3,k_4)$ according to the PWM duty-cycles ($k_1$, $k_2$, $k_3$ and $k_4$) applied to the semiconductors, including the matrix indices (1:9,1:10) that discarded the matrix row related to $\dot{v}_o$, while (10,1:10) considered it.

Considering the dc sources, the state space matrices are calculated as $\boldsymbol{A}_{fc} = \boldsymbol{A}_{fc0} + k_{fc}\boldsymbol{A}_{fck}$ for the FC and $\boldsymbol{A}_{utility} = \boldsymbol{A}_{utility0} + k_{utility}\boldsymbol{A}_{utilityk}$ for the dc utility. In this set of matrices, the matrix indices (1,1:2) select the row related to dc-link voltage, while (2,1:2) avoid it. Aiming at the input matrices from the redundancy-based dc MG model, $\boldsymbol{B}_{cb}(k_1,k_2,k_3,k_4)$ represents the model for the CBC and CBB, while $\boldsymbol{B}_{fc} = \boldsymbol{B}_{fc0} + k_{fc}\boldsymbol{B}_{fck}$ and $\boldsymbol{B}_{utility} = \boldsymbol{B}_{utility0} + k_{utility}\boldsymbol{B}_{utilityk}$ are the input matrices for the FC and dc utility. In the input matrices for the FC and dc utility, the indices (2,1) neglected the parameters related to $\dot{v}_o$, while (1,1) consider them. Finally, the current gain sensors are $Hi_{L1}$, $Hi_{L3}$, $Hi_{L5}$, $Hi_{L6}$, $Hi_{fc}$ and $Hi_{utility}$, while $\left(2\frac{v_o}{R_oC_o}\right)$ removes the redundant integration among FC, dc utility and CBC converters.

### A. Behavior of the Eigenvalues at Different Scenarios of Analysis

In the study of stability, the movement of the eigenvalues is calculated according to the Jacobian applied in the matrix (9) and then the maximum real part of the eigenvalues $max(Re(\lambda_i))$ is evaluated. In this analysis, four scenarios were examined by considering combinations of variations in a pair of parameters: the first scenario involved varying $v_{DC0\_o}$ and $v_{DC0\_C3}$, as shown in Fig. 7(a). The second scenario integrated $\alpha_{sig\_cuk}$ and $\alpha_{sig\_boost}$ variations, as shown in Fig. 7(b). In sequence, Fig. 7(c) represents the influence of the dc source parameters ($\alpha_{droop\_fc}$ and $\alpha_{droop\_utility}$), while Fig. 7(d) analyzes SoC equalization (represented by $\Delta$SoC $\rightarrow 0$) during load maneuvers.

Taking into account all subplots in Fig. 7, when the parameters are not under analysis, they are set as constants according to the following definitions: $v_{DC0\_o} = 250$ V, $v_{DC0\_C3} = 150$ V, $\alpha_{sig\_cuk} = \alpha_{sig\_boost} = 5$ (A/p.u.), $\alpha_{droop\_fc} = \alpha_{droop\_utility} = 10$ (A/p.u.), $P_{load} = 200$ W, $\text{SoC}_1 = 80\%$ and $\text{SoC}_1 = 20\%$. According to the obtained results, the system is stable because the $max(Re(\lambda_i))$ is negative (on the left side of the complex plane) in the complete analysis.

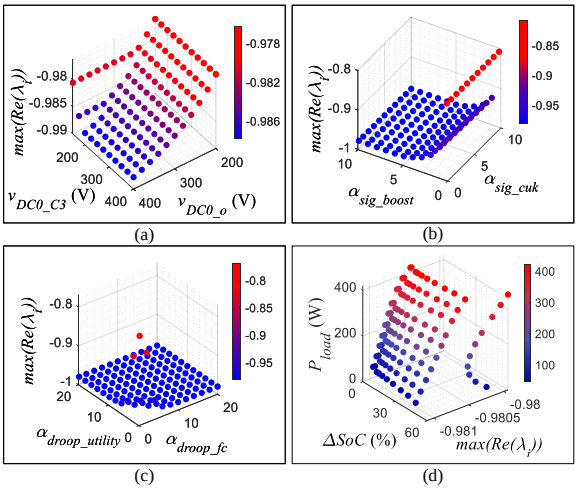


Fig. 7. Movement of $max(Re(\lambda_i))$: (a) considers dc-link variation ($v_{DC0\_o}$ and $v_{DC0\_C3}$), (b) applies SoC-Sharing variation ($\alpha_{sig\_cuk}$ and $\alpha_{sig\_boost}$), (c) evaluates optimal parameters from droop control in EMS of dc utility and FC ($\alpha_{droop\_utility}$ and $\alpha_{droop\_fc}$) and (d) load variation on dc-link as a function of $max(Re(\lambda_i))$ and equalization process when $\Delta$SoC $\rightarrow 0$.

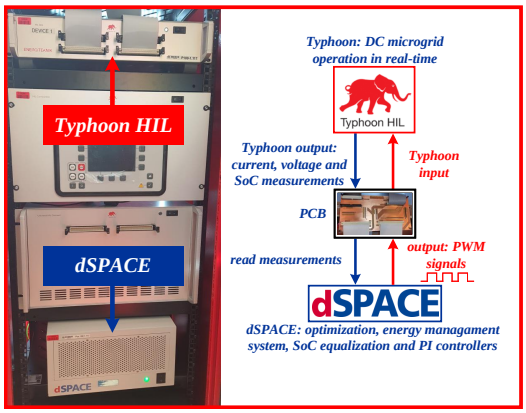


Fig. 8. HIL test model platform with the diagram showing the interaction between dSPACE and Typhoon HIL.

## VI. Experimental Results

In the experimental results, the Typhoon HIL system provides the real-time performance of the redundancy-based dc MG, while the dSPACE is responsible for sending the PWM signals calculated by the controllers according to the optimal operation mode of the EMS. The HIL test platform is showed on Fig. 8, which includes a diagram depicting the interaction between the setups through a printed circuit board (PCB).

The FC has the same parameters of H-1000 FC from Horizon Technologies with a rated power of 1 kW and 20 A as maximum current, while BESS is composed by a battery pack of Li-Po batteries with a rated capacity of 60 Ah, $\eta_{ch} = 95\%$, $\eta_{dis} = 95\%$, rated voltage of 36 V and maximum current supplied/absorbed as 10 A. In addition, the dc utility is represented by an additional dc source with 36 V and maximum current of 20 A, the switching frequency is 20 kHz and the dc-link voltage range $\Delta v$ is set to 15 V.

Considering the PSO, $\Delta t_{opt}$ = 9.6 s with a population of 25 individuals and 15 iterations. In order to reduce the impact on the FC current dynamics, its droop control requires 1.2 s to change smoothly through gradual implementation, thus minimizing the effect on its internal membranes. Furthermore, Table I shows the values designed as constraints to the PSO, which they are based on the redundancy-based dc MG operational conditions and their limitations.

### A. MG Evaluation with Load Maneuvers and failure in BESS1

The redundancy-based dc MG operates according to the real-time pricing for the $H_2$ and the electricity in the period of 3 h, as showed in Fig. 9. In this scenario, the initial SoC levels for the BESS units are $\text{SoC}_1 = 90\%$ and $\text{SoC}_2 = 10\%$, there are steps of load on the main dc-link, and BESS1 failure between 0.6 and 0.8 h. Although the PSO algorithm may require more time to reach convergence due to the EMS parameters being updated during each $\Delta t_{opt}$, the EMS effectively manages the redundancy-based dc MG by keeping its dynamics capable of handling load variations.

Evidently, $i_{L1}$ and $i_{L3}$ follow the load maneuver on dc-link because the SoC-Sharing function is responsible to provide more current when the load increase. Conversely, $i_{L5}$ and $i_{L6}$ are operating only with the optimal parameters calculated by the PSO because there is no load tied on $C_3$. Therefore, both currents go to zero when BESS1 enters the process of failure.

In addition, $i_{utility}$ and $i_{fc}$ remain able to respond the changes produced by the events in the main dc-link, while they are adjusted based on real-time pricing of $\beta_{elec}$, $\beta_{H_2}$ and the constraints outlined in Table I. In terms of the dc-link voltages $v_{C3}$ and $v_o$, there is no significant voltage deviation with load maneuvers or BESS1 failure.

Furthermore, the SoCs of the BESS units continue the balancing process, with $\text{SoC}_1$ remaining constant when BESS1 is under failure. In sequence, the BESS units approach 30% towards the end of the redundancy-based dc MG operation at 3 h. Finally, the comparison between the total operating cost is depicted in Fig. 10 when the authors are utilizing PSO, and when they are not employing any method of optimization.

TABLE I
Value of the Parameters Set on the PSO Constraints.

| | | | |
|---|---|---|---|
| $I_{bat}^{min}$ and $SoC^{min}$ | -10 A<br>10% | $I_{bat}^{max}$<br>$SoC^{max}$ | 10 A<br>90% |
| $\lvert\nabla P_{BESS}\rvert$ | 15 W | - | - |
| $V_o^{min}$ | 200 V | $V_o^{max}$ | 415 V |
| $V_{C3}^{min}$ | 150 V | $V_{C3}^{max}$ | 165 V |
| $P_{fc}^{min}$ | 0 W | $P_{fc}^{max}$ | 250 W |
| $P_{utility}^{min}$ | 0 W | $P_{utility}^{max}$ | 250 W |
| $\xi^{min}$ | 100 W | $\xi^{max}$ | 500 W |
| $P_{load}^{min}$ | 100 W | $P_{load}^{max}$ | 300 W |
| $V_{DC0\_o}^{min}$ | 200 V | $V_{DC0\_o}^{max}$ | 400 V |
| $V_{DC0\_C3}^{min}$ | 150 V | $V_{DC0\_C3}^{max}$ | 400 V |
| $\alpha_{sig\_cuk}^{min}$ | 0 A/p.u. | $\alpha_{sig\_cuk}^{max}$ | 10 A/p.u. |
| $\alpha_{sig\_boost}^{min}$ | 0 A/p.u. | $\alpha_{sig\_boost}^{max}$ | 10 A/p.u. |
| $\alpha_{droop\_fc}^{min}$ | 0 A/p.u. | $\alpha_{droop\_fc}^{max}$ | 20 A/p.u. |
| $\alpha_{droop\_utility}^{min}$ | 0 A/p.u. | $\alpha_{droop\_utility}^{max}$ | 20 A/p.u. |

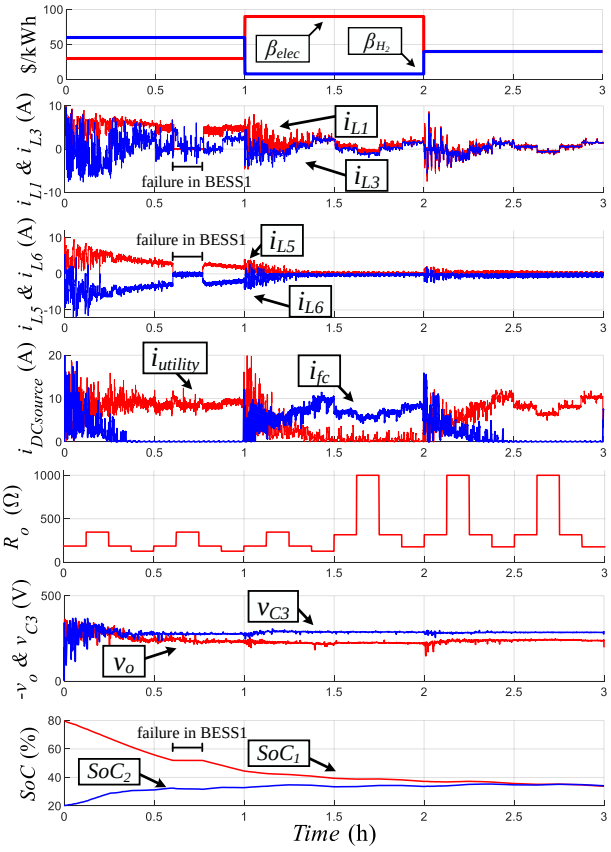


Fig. 9. MG under operation from top to bottom: real-time pricing ($\beta_{elec}$ and $\beta_{H_2}$), current inductances ($i_{L1}$, $i_{L3}$, $i_{L5}$ and $i_{L6}$), FC and the dc utility currents ($i_{fc}$ and $i_{utility}$), dc-link voltages ($v_o$ and $v_{C3}$), load variation ($R_o$) with steps at 0.125 h and the SoC equalization process.

### B. Redundancy-based constraint designed for the dc MG operation under real-time pricing

In this analysis, the load is constant (400 Ω), the initial values of SoC are $\text{SoC}_1 = 90\%$, $\text{SoC}_2 = 10\%$ and the real-time pricing is indicated in Fig. 11. Taking into account the data from Table I, the redundancy-based constraint function $v_{bat1}i_{L1} + v_{bat2}i_{L3} \leq 30$ W is addressed on the PSO, which starts at 1 h and ends at 2 h. Thus, the SoC equalization should occur through the CBC and CBB from 0 h to 1 h and then through the CBB from 1 h to 2 h. In this context, the complete test process is evaluated in Fig. 11(a), considering the SoC-Sharing function optimized via PSO. Fig. 11(b) presents a contrast with the SoC-Sharing function enhanced using the GA algorithm. Finally, an additional comparison is illustrated in Fig. 11(c), where the conventional SoC based droop is refined via PSO method (SoC based droop proposed in [6]).

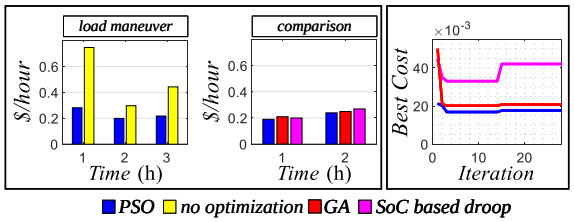


Fig. 10. Comparison of the operation cost taking into account four levels of analysis, one considering the PSO with SoC-Sharing function (proposed approach), the second without optimizing the parameters, the third based on the GA and the SoC-Sharing function and the latest based on the PSO and SoC based droop. It also presents the best cost vs. iterative cycle for each optimization as compared across each experimental result.

For achieving the GA convergence, the number of population has to be increased from 25 to 40. Consequently, the $\Delta t_{opt}$ is reduced from 9.6 s to 6 s which also decrease the gradient time of the FC droop control parameters from 1.2 s to 0.75 s. In addition, the comparison of total operating costs among each method is shown in Fig. 10, and also the best cost for each iterative cycle, highlighting the significance of the proposed method.

*1) Comparison between PSO and GA:* considering Fig. 11(b), it is evident that there are some individuals from the GA population that fails to achieve the convergence, resulting in more spikes in the behavior of $i_{L1}$, $i_{L3}$, $i_{L5}$, $i_{L6}$, $i_{fc}$ and $i_{utility}$ when the GA is compared with the PSO in Fig. 11(a).

In addition, as the both methods present similar characteristics in their operation cost, another optimization method would present similarities. Therefore, in order to classify the best approach between PSO and GA, it is possible to incorporate the dynamics derived from the operation of the redundancy-based dc MG to alleviate stress on the BESS and FC, and the best cost in the objective function regarding iterative cycles, as indicated in Fig. 10. In terms of implementation, the GA convergence was achieved with a higher number of individuals compared to PSO, which leads to a reduction in the optimization time step that may also impact the dynamics of redundancy-based dc MG.

*2) Comparison between SoC-Sharing function and traditional SoC based droop:* the BESS units take a longer period of time to achieve SoC balancing when applying the SoC based droop method in the PSO instead of the SoC-Sharing function, as shown in Fig. 11(c).

Another disparity between the two approaches is the successful operation of the redundancy-based constraint within the SoC-Sharing function between 1 h and 2 h, while the power demand remains confined to $i_{fc}$ and $i_{utility}$ in the SoC based droop method, as depicted in Fig. 11(c). As a consequence, the currents $i_{L5}$ and $i_{L6}$ are significantly high enough to facilitate SoC equalization in the SoC-Sharing function when compared to the SoC based droop. Additionally, the best cost at each iterative cycle is higher for the SoC based droop than for the proposed approach, as indicated in Fig. 10.

## VII. Conclusion

This paper introduces a novel approach utilizing a PSO algorithm to enhance the EMS responsible for coordinating dc utility, FC and BESS units. The proposed methodology involves gathering measurements from a redundancy-based dc MG, followed by deriving optimal parameters that improve the performance of the droop control and SoC-Sharing function align with electricity and $H_2$ costs. Consequently, the economic operational expenses of the redundancy-based dc MG

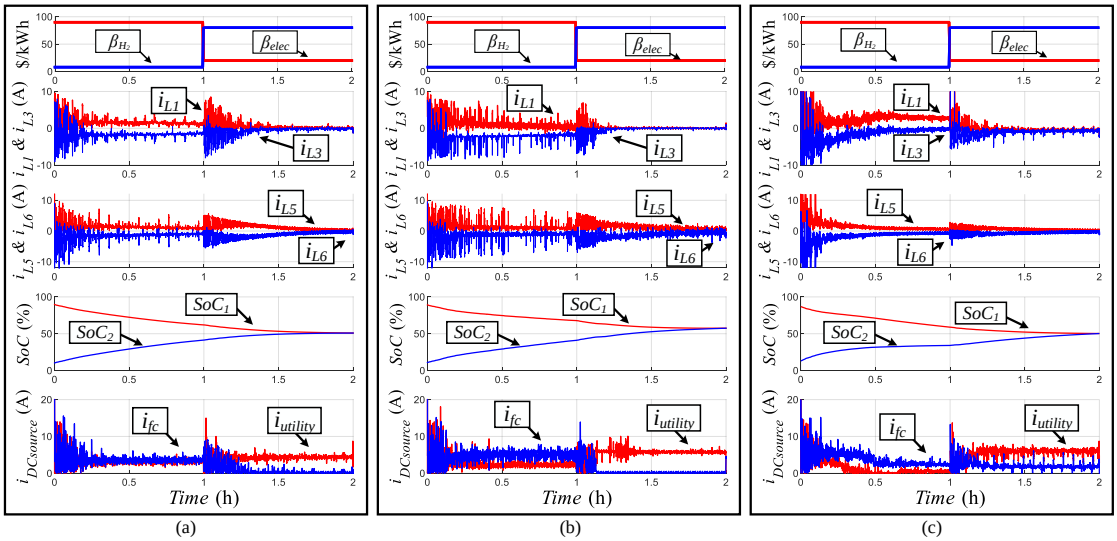


Fig. 11. MG under operation at constant load with 400 Ω. Real-time pricing ($\beta_{elec}$ and $\beta_{H_2}$), current inductances ($i_{L1}$, $i_{L3}$, $i_{L5}$ and $i_{L6}$), SoC equalization behavior, FC current and dc utility current ($i_{fc}$ and $i_{utility}$): (a) SoC-Sharing function optimized by PSO. (b) SoC-Sharing function optimized by GA. (c) SoC based droop optimized by PSO.

are reduced, and system efficiency is increased by factoring in power electronics losses within the optimization process.

Furthermore, the integration of the PSO algorithm with the dc MG configuration allows the use of redundant modules, including CBC and CBB, during the SoC equalization process. The paper also outlines the redundancy-based dc MG topology, introduces the PSO approach for optimizing droop control and SoC-Sharing function, and subsequently employs Lyapunov's indirect method to establish the stability of the proposed structure. Experimental results are presented to validate the effectiveness of the proposed approach.

Importantly, the utilization of the PSO algorithm significantly reduces the overall operational cost when compared to an EMS operating without any optimization strategy. In comparison to the GA approach, PSO leads to lower stress levels on BESS units and FC, and stands out for its easier implementation. Furthermore, when compared to the conventional SoC based droop, the SoC-Sharing function achieves a faster balance in the SoC of the BESS units. As a potential direction for future research, the consideration of the SoH could be integrated into the operation of the redundancy-based dc MG. This integration would involve assessing the operation related to SoC equalization among BESS units.

## REFERENCES


[1] N. Salehi, H. Martínez-García, G. Velasco-Quesada, and J. M. Guerrero, "A comprehensive review of control strategies and optimization methods for individual and community microgrids," *IEEE Access*, vol. 10, pp. 15 935–15 955, 2022.

[2] L. Che, M. Shahidehpour, A. Alabdulwahab, and Y. Al-Turki, "Hierarchical coordination of a community microgrid with ac and dc microgrids," *IEEE Transactions on Smart Grid*, vol. 6, no. 6, pp. 3042–3051, 2015.

[3] J. Wang, Z. Liu, J. Liu, and T. Wu, "A mode switching-based decentralized secondary control for microgrids with hybrid droop and master-slave structure," *IEEE Open Journal of Power Electronics*, vol. 3, pp. 334–347, 2022.

[4] E. Espina, J. Llanos, C. Burgos-Mellado, R. Cárdenas-Dobson, M. Martínez-Gómez, and D. Sáez, "Distributed control strategies for microgrids: An overview," *IEEE Access*, vol. 8, pp. 193 412–193 448, 2020.

[5] T. A. Fagundes, G. H. F. Fuzato, C. R. De Aguiar, K. D. A. Ottoboni, M. Biczkowski, and R. Q. Machado, "Management and equalization of energy storage devices for dc microgrids using a soc-sharing function," *IEEE Access*, vol. 8, pp. 78 576–78 589, 2020.

[6] Y. Xia, M. Yu, P. Yang, Y. Peng, and W. Wei, "Generation-storage coordination for islanded dc microgrids dominated by pv generators," *IEEE Transactions on Energy Conversion*, vol. 34, no. 1, pp. 130–138, 2019.

[7] G. Tian, Y. Zheng, G. Liu, and J. Zhang, "SOC balancing and coordinated control based on adaptive droop coefficient algorithm for energy storage units in dc microgrid," *Energies*, vol. 15, no. 8, 2022.

[8] D. I. Brandao, R. P. d. Santos, W. W. A. G. Silva, T. R. Oliveira, and P. F. Donoso-Garcia, "Model-free energy management system for hybrid alternating current/direct current microgrids," *IEEE Transactions on Industrial Electronics*, vol. 68, no. 5, pp. 3982–3991, 2021.

[9] T. A. Fagundes, G. H. F. Fuzato, P. G. B. Ferreira, M. Biczkowski, and R. Q. Machado, "Fuzzy controller for energy management and soc equalization in dc microgrids powered by fuel cell and energy storage units," *IEEE Journal of Emerging and Selected Topics in Industrial Electronics*, vol. 3, no. 1, pp. 90–100, 2022.

[10] T. R. Oliveira, W. W. A. Gonçalves Silva, and P. F. Donoso-Garcia, "Distributed secondary level control for energy storage management in dc microgrids," *IEEE Transactions on Smart Grid*, vol. 8, no. 6, pp. 2597–2607, 2017.

[11] C. Li, F. de Bosio, F. Chen, S. K. Chaudhary, J. C. Vasquez, and J. M. Guerrero, "Economic dispatch for operating cost minimization under real-time pricing in droop-controlled dc microgrid," *IEEE Journal of Emerging and Selected Topics in Power Electronics*, vol. 5, no. 1, pp. 587–595, 2017.

[12] Z. Fan, B. Fan, J. Peng, and W. Liu, "Operation loss minimization targeted distributed optimal control of dc microgrids," *IEEE Systems Journal*, vol. 15, no. 4, pp. 5186–5196, 2021.

[13] B. Abdolmaleki and G. Bergna-Diaz, "Distributed control and optimization of dc microgrids: A port-hamiltonian approach," *IEEE Access*, vol. 10, pp. 64 222–64 233, 2022.

[14] S. Wang, M. Du, L. Lu, W. Xing, K. Sun, and M. Ouyang, "Multilevel energy management of a dc microgrid based on virtual-battery model considering voltage regulation and economic optimization," *IEEE Journal of Emerging and Selected Topics in Power Electronics*, vol. 9, no. 3, pp. 2881–2895, 2021.

[15] J. Peng, B. Fan, and W. Liu, "Voltage-based distributed optimal control for generation cost minimization and bounded bus voltage regulation in

dc microgrids," *IEEE Transactions on Smart Grid*, vol. 12, no. 1, pp. 106–116, 2021.
[16] S. Fang, Y. Xu, H. Wang, C. Shang, and X. Feng, "Robust operation of shipboard microgrids with multiple-battery energy storage system under navigation uncertainties," *IEEE Transactions on Vehicular Technology*, vol. 69, no. 10, pp. 10 531–10 544, 2020.
[17] R. Faraji, L. Ding, T. Rahimi, and M. Kheshti, "Application of soft-switching cell with inherent redundancy properties for enhancing the reliability of boost-based dc–dc converters," *IEEE Transactions on Power Electronics*, vol. 36, no. 11, pp. 12 342–12 354, 2021.
[18] W. Zhang, D. Xu, P. N. Enjeti, H. Li, J. T. Hawke, and H. S. Krishnamoorthy, "Survey on fault-tolerant techniques for power electronic converters," *IEEE Transactions on Power Electronics*, vol. 29, no. 12, pp. 6319–6331, 2014.
[19] M. Farhadi and O. Mohammed, "Adaptive energy management in redundant hybrid dc microgrid for pulse load mitigation," *IEEE Transactions on Smart Grid*, vol. 6, no. 1, pp. 54–62, 2015.
[20] P. Chen, F. Xiao, J. Liu, Z. Zhu, and Q. Ren, "Unbalanced operation principle and fast balancing charging strategy of a cascaded modular multilevel converter–bidirectional dc–dc converter in the shipboard applications," *IEEE Transactions on Transportation Electrification*, vol. 6, no. 3, pp. 1265–1278, 2020.
[21] G. H. F. Fuzato, C. R. de Aguiar, T. A. Fagundes, W. C. Leal, J. C. Vasquez, J. M. Guerrero, and R. Q. Machado, "Droop k-sharing function for energy management of dc microgrids," *IEEE Journal of Emerging and Selected Topics in Industrial Electronics*, vol. 2, no. 3, pp. 257–266, 2021.
[22] N. Li, F. Gao, T. Hao, Z. Ma, and C. Zhang, "SOH balancing control method for the MMC battery energy storage system," *IEEE Transactions on Industrial Electronics*, vol. 65, no. 8, pp. 6581–6591, 2018.
[23] J. Hu, Y. Shan, Y. Yang, A. Parisio, Y. Li, N. Amjady, S. Islam, K. W. Cheng, J. M. Guerrero, and J. Rodríguez, "Economic model predictive control for microgrid optimization: A review," *IEEE Transactions on Smart Grid*, pp. 1–1, 2023.
[24] T. A. Jumani, M. W. Mustafa, A. S. Alghamdi, M. M. Rasid, A. Alamgir, and A. B. Awan, "Swarm intelligence-based optimization techniques for dynamic response and power quality enhancement of ac microgrids: A comprehensive review," *IEEE Access*, vol. 8, pp. 75 986–76 001, 2020.
[25] M. H. Moradi, M. Eskandari, and S. Mahdi Hosseinian, "Operational strategy optimization in an optimal sized smart microgrid," *IEEE Transactions on Smart Grid*, vol. 6, no. 3, pp. 1087–1095, 2015.
[26] M. Ruiz-Cortés, E. González-Romera, R. Amaral-Lopes, E. Romero-Cadaval, J. Martins, M. I. Milanés-Montero, and F. Barrero-González, "Optimal charge/discharge scheduling of batteries in microgrids of prosumers," *IEEE Transactions on Energy Conversion*, vol. 34, no. 1, pp. 468–477, 2019.

**Thales Augusto Fagundes** was born in Jundiai, Brazil. He received the B.S. in electrical engineering in 2017 and the M.S. degree in 2020 from the University of Sao Paulo (Sao Carlos, Brazil). In 2014, he studied abroad at the University of New South Wales (Sydney, Australia), focusing on courses related to alternative energy sources. He is currently working on his Ph.D. in electrical engineering at the University of Sao Paulo and from 2022 to 2023 he was a visiting researcher at the Aalborg University. His main research interest are in the fields of microgrids, energy management and DC-DC converters for renewable energy sources and storage systems.

**Guilherme Henrique Favaro Fuzato** was born in Varginha, Brazil, in 1989. He received the B.S. in Electrical Engineering in 2011, the M.S. degree in Power Electronics and Dynamic Systems in 2015, and the Ph.D. degree in Microgrids in 2019 from University of São Paulo. From 2018 to 2019 he was a visiting researcher at the Aalborg University. From 2012 to 2013 he worked at Siemens as a field service engineer in automation area. From 2014 to 2015 he worked at Bosch with power electronics in automotive applications as a temporary researcher. Since 2016, he has been working as lecturer at the Federal Institute of Education, Science and Technology of São Paulo. His main research interests are in the fields of microgrids, energy management and DC-DC converter for renewable energy sources and storage systems.

**Rafael Fernando Quirino Magossi** received the B.Eng., M.Sc. and Ph.D. degrees in electrical engineering from the University of São Paulo, São Carlos, Brazil, in 2016, 2018 and 2020, respectively. From 2018 to 2022, he was an assistant professor at the Federal Center for Technological Education (CEFET/RJ) in Rio de Janeiro, Brazil. Since 2022, he has been the CTO at Solar21 in São Paulo, Brazil. His research interests include control systems, power electronics, and renewable power systems.

**Manuel Antonio Barrios Flores** is an electrical engineer from Mexico, has an academic and professional background in renewable energy systems, power converters, and real-time simulation. Having received his B.Eng, M.Eng, and Ph.D degrees in 2013, 2017, and 2023 respectively, he has since undertaken significant research and project work. This includes stays at LiCORE AC and Aalborg University, Denmark, where he contributed to two industrial projects with Sonnen Inc and SALICRU SA. His research interests span across a variety of areas in the field of energy technology.

**Juan C. Vasquez** (Senior Member, IEEE) received the B.Sc. and Ph.D. degrees from UAM, Colombia, and the Ph.D. degree from UPC, Spain. In 2019, he was a Professor of energy internet and microgrids. He is currently the Co-Director of the Villum Center for Research on Microgrids. He has published more than 450 journal articles cited more than 30000 times. His research interests include operation, control, energy management applied to ac/dc microgrids, the integration of IoT, energy internet, digital twin, and blockchain solutions. He has been awarded as a Highly Cited Researcher, since 2017. He was a recipient of the Young Investigator Award, in 2019.

**Josep M. Guerrero** (Fellow, IEEE) received the B.S. degree in telecommunications engineering, the M.S. degree in electronics engineering, and the Ph.D. degree from the Technical University of Catalonia, Barcelona, in 1997, 2000, and 2003, respectively. In 2019, he was a Villum Investigator at the Villum Fonden, which supports the Center for Research on Microgrids (CROM), Aalborg University, Denmark. Since 2011, he has been a Full Professor with the Department of Energy Technology, Aalborg University. His research interests include different microgrid aspects, including applications as remote communities, energy prosumers, and maritime and space microgrids.

**Ricardo Quadros Machado** (M'2005, SM'2018) was born in Santa Maria, Brazil. He received the B. S. from the University of Santa Maria (Santa Maria, Brazil) in 1997, the M.S. (2000) and the Ph.D. (2005) degrees in Electrical Engineering from the University of Campinas (Campinas, Brazil). From 2002 to 2003 he was a visiting researcher at the University of Padova (Padova, Italy) and from 2005 to 2007 he was a post-doctorate at the Federal University of Santa Maria, (Santa Maria, Brazil). From 2013 to 2014 he was visiting professor at the University of Toronto (Toronto, Canada). Additionally, from 2007 to 2018 he was assistant professor at the University of São Paulo (São Carlos, Brazil). Currently, he is associated professor at the University of São Paulo (São Carlos, Brazil) and his main research interests are: processing of energy in dc/dc and dc/ac converters, digital control of power converters, distributed generation systems, smart grids and control of renewable energy sources.